GAUSSIAN MIXTURE CONVOLUTION NETWORKS

Anonymous authors
Paper under double-blind review

ABSTRACT

This paper proposes a novel method for deep learning based on the analytical convolution of multidimensional Gaussian mixtures. In contrast to tensors, these do not suffer from the curse of dimensionality and allow for a compact representation, as data is only stored where details exist. Convolution kernels and data are Gaussian mixtures with unconstrained weights, positions, and covariance matrices. Similar to discrete convolutional networks, each convolution step produces several feature channels, represented by independent Gaussian mixtures. Since traditional transfer functions like ReLUs do not produce Gaussian mixtures, we propose using a fitting of these functions instead. This fitting step also acts as a pooling layer if the number of Gaussian components is reduced appropriately. We demonstrate that networks based on this architecture reach competitive accuracy on Gaussian mixtures fitted to the MNIST and ModelNet datasets.

1 INTRODUCTION

Convolutional neural networks (CNNs) have led to the widespread adoption of deep learning in many disciplines. They operate on grids of discrete data samples, i.e., vectors, matrices, and tensors, which are structured representations of data. While this is approach is sufficiently efficient in one and two dimensions, it suffers the curse of dimensionality: The amount of data is $O(d^k)$, where d is the resolution of data, and k is the dimensionality. The exponential growth permeates all layers of a CNN, which must be scaled appropriately to learn a sufficient number of k-dimensional features. In three or more dimensions, the implied memory requirements thus quickly become intractable (Maturana & Scherer, 2015; Zhirong Wu et al., 2015), leading researchers to propose specialized CNN architectures as a trade-off between mathematical exactness and performance (Riegler et al., 2017; Wang et al., 2017). In this work, we propose a novel deep learning architecture based on the analytical convolution of Gaussian mixtures (GMs). While maintaining the elegance of conventional CNNs, our architecture does not suffer from the curse of dimensionality and is therefore well-suited for application to higher-dimensional problems.

GMs are inherently unstructured and sparse, in the sense that no storage is required to represent empty data regions. In contrast to discretized k-dimensional volumes, this allows for a more compact representation of data across dimensions, preventing exponential memory requirements. In this regard, they are similar to point clouds (Qi et al., 2017a). However, GMs also encode the notion of a spatial extent. The fidelity of the representation directly depends on the number of Gaussians in the mixture, which means that, given an adequate fitting algorithm and sufficient resources, it can be arbitrarily adjusted. Hence, GMs allow trading representation accuracy for memory requirements on a more fine-grained level than voxel grids.

In this work, we present our novel architecture, the *Gaussian mixture convolution network* (GMCN), as an alternative to conventional CNNs. An important distinguishing feature of GMCNs is that both, data and learnable kernels, are represented using mixtures of Gaussian functions. We use Gaussians with unconstrained weights, positions, and covariances, enabling the mixtures to adapt more accurately to the shape of data than a grid of discrete samples could. Unlike probability models, our approach supports negative weights, which means that arbitrary data can be fitted. Especially for sparse data sets and problems, such a representation can lead to considerable memory savings.

At their core, CNNs are deep neural networks, where each pixel or voxel is a neuron with distinct connections to other neurons, with shared weights and biases. On the other hand, GMCNs represent data as functions. Hence there are no distinct neurons, and the concept of connection does not exist. Our architecture could thus be more appropriately classified as a *deep functional network*.

Like conventional (discrete) CNNs, our proposed GM learning approach supports several convolution layers, an increasing number of feature channels, and pooling, in order to learn and detect aspects of the input. For the convolution of two mixtures, a closed-form solution is used, which results in a new mixture. Conventional transfer functions like ReLUs do not produce a GM. However, a GM is required to feed the next convolution layer in a deep network. Therefore, we propose to *fit* a GM to the result of the transfer function. The fitting process can simultaneously act as a pooling layer if the number of fitted components is reduced appropriately in successive convolution layers. Unlike most point convolutional networks, which have per-point feature vectors, the feature channels of GMCNs are not restricted to share the same positions or covariance matrices.

With the presentation of GMCNs, we thus provide the following scientific contributions:

- A deep learning architecture based on the analytical convolution of Gaussian mixtures.
- A heuristic for fitting a Gaussian mixture to the result of a transfer function.
- A fitting method to both reduce the number of Gaussians and act as a pooling layer.
- A thorough evaluation of GMCNs, including ablation studies.

2 Related work

CNNs have been successfully applied to images (e.g., Krizhevsky et al. (2012)) and small 3D voxel grids (e.g., Maturana & Scherer (2015), and Ji et al. (2013)). However, it is not trivial to apply discrete convolution to large 3- or more dimensional problems due to the dimensional explosion. Riegler et al. (2017) reduce memory consumption by storing data in an octree, but the underlying problem remains.

GMs have been used in 3D computer graphics, e.g., by Jakob et al. (2011) for approximating volumetric data, and by Preiner et al. (2014) and Eckart et al. (2016a) for a probabilistic model of point clouds. In particular, the work by Eckart et al. can be used to fit GMs to point clouds, which can then be used as input to our network (see ablation study in Section 5.3). We use the expectation-maximization (EM) algorithm proposed by Dempster et al. (1977) to fit input data, and EM equations for fitting small GMs to larger ones by Vasconcelos & Lippman (1999).

We refer to Ahmed et al. (2018) for a general overview of deep learning on 3D data. Like point clouds, GMs are unordered but with additional attributes (weight and covariance). These additional attributes could be processed like feature vectors attached to points. Therefore, prior work on point clouds is relevant, whereby Guo et al. (2019) provide a good overview.

Several authors propose point convolutional networks, e.g., Li et al. (2018b), Xu et al. (2018), Hermosilla et al. (2018), Thomas et al. (2019), Boulch (2019), and Atzmon et al. (2018). The one by Atzmon et al. is most similar to ours. They add a Gaussian with uniform variance for every point, creating a mixture that is a coarse fitting of the point cloud. After analytical convolution, the result is sampled at the original locations of the point cloud. However, information away from these points is lost. Effectively, such a restricted convolution creates a weighting function for neighboring points.

Radial Basis Function Networks also learn a GM to detect patterns on the input data (Broomhead & Lowe, 1988). However, the goal of such networks differs from our approach. While their goal is, similar to MLPs, to detect patterns on a set of data points, our method uses radial basis functions to detect patterns using a convolution operator on another set of radial basis functions.

3 Gaussian mixtures and convolution in multiple dimensions

A multidimensional Gaussian function is defined as

$$\mathrm{g}(\boldsymbol{x}, a, \boldsymbol{b}, C) = \frac{a}{\sqrt{(2\pi)^k \det(C)}} e^{-\frac{1}{2}(\boldsymbol{x}-\boldsymbol{b})^T C^{-1} (\boldsymbol{x}-\boldsymbol{b})}, \tag{1}$$

where k is the number of dimensions, a the weight, $\boldsymbol{b}$ the shift or centre point, and C the shape (covariance matrix) of the Gaussian. A GM is the sum of multiple such Gaussians:

$$\mathrm{gm}(\boldsymbol{x}, \boldsymbol{a}, B, \boldsymbol{C}) = \sum_{i=0}^{N} \mathrm{g}(\boldsymbol{x}, \boldsymbol{a}_i, B_i, \boldsymbol{C}_i) \tag{2}$$

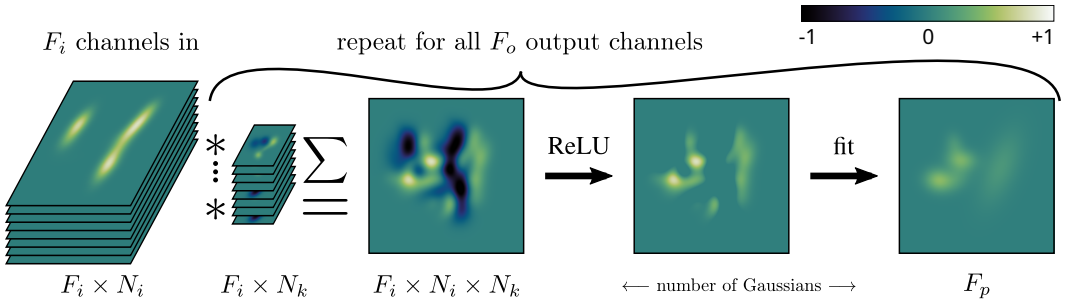

Figure 1: Design of a Gaussian convolution layer: The inputs are F_i channels of GMs with N_i components each, which are analytically convolved with F_i learnable kernels, N_k components each. The convolved mixture contains $F_i \times N_i \times N_k$ components. After applying the ReLU, a GM with N_p components is fitted. This is repeated for all of the F_o output feature channels. The resulting tensor becomes the input of the next convolution channel, with the number of output channels F_o becoming F_i, and N_p becoming N_i. The fitting must be fully differentiable with respect to the input of the ReLU. In this example, $F_i = 8$, $N_i = 16$, $N_k = 5$, and $N_p = 8$.

A GM is not a probabilistic model since the weights $\boldsymbol{a}$ can be negative and do not necessarily sum up to 1. The convolution of two Gaussians according to Vinga (2004) is given by

$$\mathrm{g}(\boldsymbol{x}, a, \boldsymbol{b}, C) * \mathrm{g}(\boldsymbol{x}, \alpha, \boldsymbol{\beta}, \Gamma) = \mathrm{g}\left(\boldsymbol{x}, a\alpha, \boldsymbol{b} + \boldsymbol{\beta}, C + \Gamma\right). \tag{3}$$

Due to the distributive property of convolution, we have:

$$\sum_{n=0}^{N} \mathrm{g}_n(\boldsymbol{x}) * \sum_{m=0}^{M} \mathrm{g}_m(\boldsymbol{x}) = \sum_{n=0}^{N} \sum_{m=0}^{M} \mathrm{g}_n(\boldsymbol{x}) * \mathrm{g}_m(\boldsymbol{x}), \tag{4}$$

where $\mathrm{g}_i(\boldsymbol{x})$ is a short hand for $\mathrm{g}(\boldsymbol{x}, \boldsymbol{a}_i, B_i, \boldsymbol{C}_i)$. Clearly, the convolution of one mixture with N terms with another mixture with M terms yields a mixture with $N \times M$ terms.

4 Gaussian Mixture Convolution Networks

Conventional CNNs typically consist of several feature channels, convolution layers, a transfer function, and pooling layers. In this section, we will show that all these components can be implemented by GMCNs as well. As a result, our overall architecture is similar to discrete CNNs, except that data and kernels are represented by Gaussian functions rather than pixels or voxels.

Convolution layer. All batch elements and feature channels contain the same number of components, allowing for packing Gaussian data (i.e., weights, positions, and covariances) into a single tensor. Like in conventional CNNs, each output channel (F_o) in a GMCN is the sum of all F_i input channels, convolved with individual kernels (Figure 1). In practice, this means that multiple convolution results are concatenated in the convolution layer. This results in a mixture with $N_o = F_i N_i N_k$ components, where N_i and N_k are the number of Gaussians in the input and kernel mixtures, respectively.

Transfer function. The ReLU is a commonly used transfer function, whose ramp-like shape is defined by $\varphi(x) = \max(0, x)$. When applying this transfer function to a mixture gm, we get

$$\varphi(\mathrm{gm}(\boldsymbol{x})) = \max(0, \sum_{n=0}^{N_o} \mathrm{g}_n(\boldsymbol{x})). \tag{5}$$

We can use Equation 5 to evaluate the mixture at particular locations of $\boldsymbol{x}$, as shown in Figure 2b. However, any subsequent convolution layers in a GMCN will again require a GM as input. Another problem inherent to the definition of GM convolution in Section 3, is that the number of intermediate output components (and thus implied memory requirements of hidden layers) is set to increase with each convolution. We address both of these problems by introducing a dedicated fitting step that produces a new, smaller mixture to represent the result of $\varphi(\mathrm{gm}(\boldsymbol{x}))$ and act as input for subsequent GMCN layers.

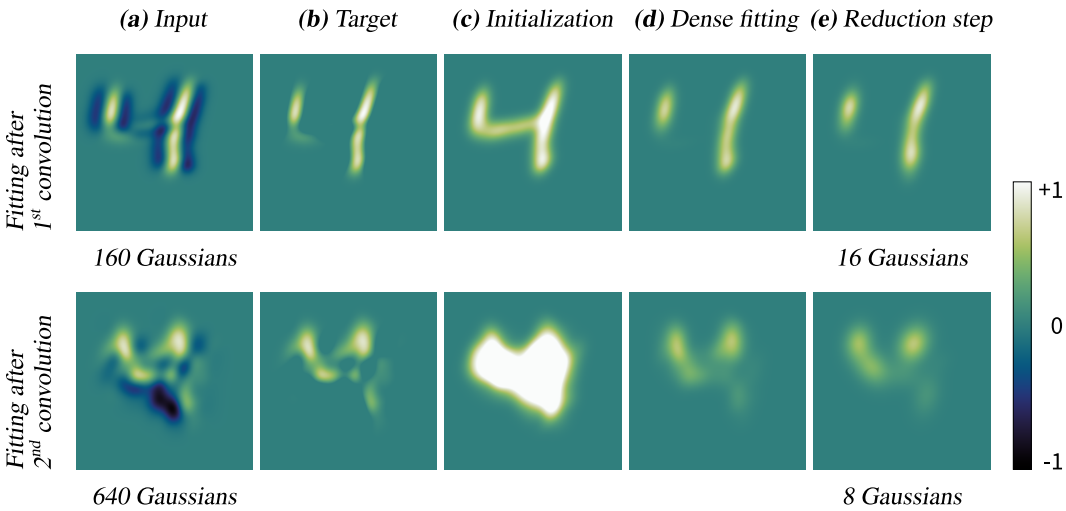

Figure 2: Examples of the fitting pipeline described in Section 4.1: The input mixture is shown in (a) and in (b) after applying the ReLU. (c) and (d) show the coarse approximation (a') and final weights (a'') of the dense fitting. The mixture after the reduction step is shown in (e). The overall fitting error is bound by dense fitting, as theoretically, reduction can be omitted altogether (or a very high number of Gaussians used).

4.1 Gaussian mixture fitting

Fitting a GM to the output of the transfer function is not trivial. In order to propagate the gradient to the kernels, the fitting method must be differentiable with respect to the parameters of the Gaussian components in gm. We decided to first fit a dense GM to the transfer function output (e.g., a ReLU $\varphi(\mathrm{gm}(\boldsymbol{x}))$, shown in Figure 2b), and then reduce the number of Gaussians in a separate step.

Dense fitting. To reduce the degrees of freedom that we must optimize for during fitting, we first assume that some Gaussians in the output of the last convolution step are meaningfully placed. Hence, we freeze their positions and adjust only their weights. One possible solution to adjust the GM's weights would be to set up an overdetermined linear system, defined by a set of sample points in the mixture and the corresponding output values. This set of equations could then be fed to a solver for determining the optimal GM weights to fit the outputs according to least squares. However, our experiments have shown that this approach quickly becomes intractable, as it requires too many samples to achieve a fitting that is both stable wrt. their selection and generalizes well to locations that lie between selected points (see Appendix C for details).

To avoid the implied restrictive memory overhead and severe bottleneck it would cause, we chose to pursue a less resource-heavy solution and propose the following heuristic instead: First, a coarse approximation ($\boldsymbol{a'}$) of the new weights is computed according to

$$\boldsymbol{a'_i} = \begin{cases} \boldsymbol{a_i}, & \text{if } \boldsymbol{a_i} > 0 \\ \epsilon, & \text{otherwise} \end{cases}, \tag{6}$$

where $\boldsymbol{a_i}$ are the weights of the old mixture, and i runs through all Gaussians. The new weights $\boldsymbol{a''}$ are then computed using a correction based on the transfer function

$$\boldsymbol{a''_i} = \boldsymbol{a'_i} \times \frac{\varphi\left(\mathrm{gm}(B_i, \boldsymbol{a}, B, \boldsymbol{C})\right)}{\mathrm{gm}(B_i, \boldsymbol{a'}, B, \boldsymbol{C})}, \tag{7}$$

where B contains the positions, $\boldsymbol{C}$ the covariance matrices, and φ represents the ReLU. Effectively, the fraction computes a correction term for the coarse approximation $\boldsymbol{a'}$. It is guaranteed, that the new weights $\boldsymbol{a''}$ are positive, just like we would expect from a ReLU. Examples of the coarse approximation ($\boldsymbol{a'}$) are given in Figure 2c, and the final fitting ($\boldsymbol{a''}$) in Figure 2d. The fitting is most precise at the Gaussian centers. Problems arise at the discontinuity of the ReLU, where the result can be overly smooth, as seen in Figure 3a, or with an adverse configuration of covariances, as is the case in Figure 3b.

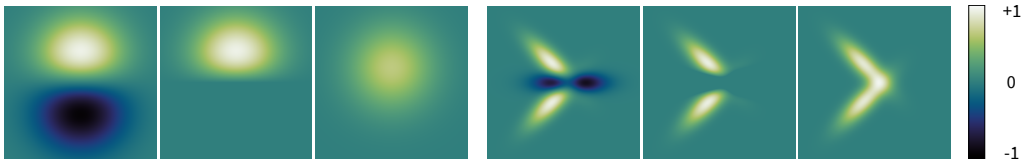

(a) *Overly smooth zero-crossing* ***(b)*** *Bad covariance configuration*

Figure 3: Failure cases for dense fitting: We show inputs, ReLU reference outputs, and our own. In (a), the zero-crossing is overly smooth, and the output weight too small. The positive Gaussian should have been moved up instead. In (b), covariances have a bad configuration, they should have been reduced, and the position moved.

Reduction step. The next step in our fitting performs expectation-maximization (EM) to reduce the number of Gaussians in the mixture. We implemented two variants, a simpler *modified EM* variant based on the derivations from Vasconcelos & Lippman (1999), and our own tree-based hierarchical EM method. For the simpler, modified EM variant, we select the N_p Gaussians with the largest integrals out of the N_o available ones. Then, one step of EM is performed, balancing accuracy with compute and memory resources, resulting in the fitting. However, this procedure implies $O(N_o \times N_p)$ in terms of memory and computation complexity, rendering it too expensive for larger mixtures.

To remedy this issue, we propose tree-based hierarchical expectation-maximization (TreeHEM). A fundamental idea of TreeHEM is to merge Gaussians in close proximity preferentially. To this end, the Gaussians are first sorted into a tree hierarchy, based on the Morton code of their position, similar to Lauterbach et al. (2009). This tree is traversed bottom-up, collecting up to $2T$ Gaussians and performing a *modified EM* step, which reduces the number to T Gaussians. The fitted Gaussians are stored in tree nodes. The process continues iteratively, collecting again up to $2T$ Gaussians followed by fitting, until we reach the root. Finally, the tree is traversed top-down, greedily collecting the Gaussians with most mass from the nodes until the desired number of fitted Gaussians is reached. Hence, TreeHEM yields an $O(N_o \log N_o)$ algorithm. We found that a value of $T = 2$ works best in terms of computation time, memory consumption, and often fitting error (Section 5.3). TreeHEM was implemented in CUDA; gradients were derived manually. Examples are shown in Figure 2e.

4.2 Regularization and maintaining valid kernels

In order to add support for regularization to the learning process, we can apply weight decay, which pushes weights towards zero and the covariance matrices towards identity:

$$d_i = a_i^2 + \text{mean}\left((C_i - I) \odot (C_i - I)\right), \tag{8}$$

where d_i is the weight decay loss for kernel Gaussian i, and a, C, and I are the weights, covariances, and the identity matrix, respectively.

Training the GMCN includes updates to the covariance matrices of kernel Gaussians. In order to prevent singular matrices, C_l is learned, and then turned into a symmetrical non-singular matrix by

$$C = {C_l}^T C_l + I\epsilon. \tag{9}$$

4.3 Pooling

In conventional CNNs, pooling merges data elements and reduces the (discrete) domain size at the same time. As filter kernels remain identical in size but are applied to a smaller domain, their receptive field effectively increases.

For pooling data with GMCNs, we can set up the fitting step (Section 4.1) such that the number of fitted Gaussians is reduced by half on each convolution layer. While this effectively pools the data Gaussians by increasing their extent, it does not scale the domain. Thus, using the same kernels on the so-fitted data does not automatically lead to an increased receptive field. To achieve this, the kernel Gaussians would have to increase in size to match the increase in the data Gaussians' extent. Instead, similar to conventional CNNs, we simply reduce the data mixtures' domain by scaling positions and covariances. We compute the scaling factor such that after each layer, the average trace of the

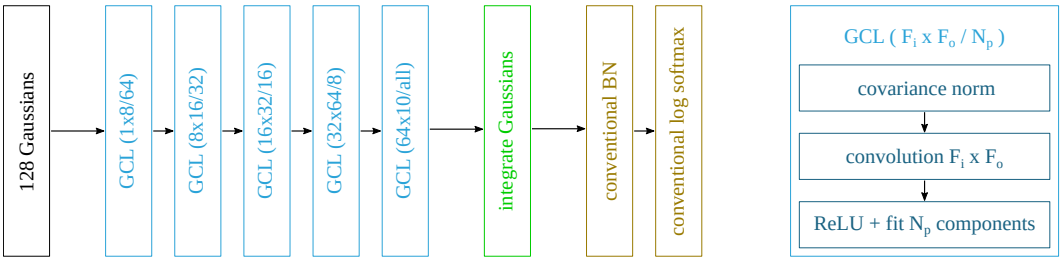

Figure 4: The GMCN used in for our evaluation uses 5 Gaussian convolution layers (GCL, see right-hand side), integration of feature channel mixtures, and conventional transfer functions. See Section 5 for more details.

covariance matrices becomes the number of dimensions (2 or 3 currently), leading to an average variance of 1 per dimension. Effectively, this leads to Gaussian centers moving closer together and covariances becoming smaller. Hence, the receptive field of each kernel becomes larger in relation to the original data scale, even if the kernel size is fixed.

5 Evaluation

To evaluate our architecture, we use the proposed GMCN architecture to train classification networks on a series of well-known tasks. We used an NVIDIA GeForce 2080Ti for training. For all our experiments, we used the same network architecture and training parameters shown in Figure 4. First, we fit a GM to each input 2D or 3D sample by using the k-means algorithm for defining the center of the Gaussians and one step of the EM algorithm to compute the covariance matrices. The mixture weights are then normalized such that the mixtures have the same activation across all training samples on average. Covariance matrices and positions are normalized using the same procedure as for pooling (Section 4.3). The input GM is then processed by four consecutive blocks of Gaussian convolution and ReLU fitting layers, where each doubles the number of feature channels and halves the number of Gaussians. The resulting numbers of channels per block are $[8, 16, 32, 64]$. Finally, an additional convolution and ReLU block outputs one feature channel per class. For performance reasons, we do not reduce the number of Gaussians in this last block. These feature channels are then integrated to generate a scalar value, which is further processed by a conventional batch-normalization layer. The resulting values are converted to probabilities by using the $\mathrm{Softmax}$ operation, from which the negative-log-likelihood loss is computed.

The kernels of each convolutional layer are represented by five different Gaussians, with weights randomly initialized from a normal distribution with variance 1.0 and mean 0.1. One Gaussian is centered at the origin, while the centroids of the remaining ones are initialized along the positive and negative x- and y-axes at a distance of 2.5 units from the origin. For the 3D case, the remaining Gaussians are placed randomly at a distance of 2.5 units from the origin. The covariance factor matrix of each Gaussian is initialized following $(I + R * 0.05) * 0.7$, where I is the identity, and R a matrix of random values in the range between -1 and 1. The covariance matrix was then computed according to Equation 9. We determined these values using a grid search. Examples of kernels are shown in Appendix A.

All models are trained using the Adam optimizer, with an initial learning rate of 0.001. The learning rate is reduced by a scheduler once the accuracy plateaus. Moreover, we apply weight decay scaled by 0.1 of the learning rate to avoid overfitting, as outlined in Section 4.2.

5.1 2D data classification (MNIST)

The MNIST data set (Lecun et al., 1998) consists of 70 K handwritten digits from 10 different classes. In this task, models have to predict the digit each image represents, where performance is measured as overall accuracy. We trained our GMCN architecture using the standard train/test splits by fitting 64 Gaussians to each image and processing them with our model. Figure 5 shows some examples of the generated GMs. Our trained model achieved an accuracy of $99.4\,\%$ on this task, which is close to the $99.8\,\%$ currently reported by other state-of-the-art methods (Byerly et al., 2020; Mazzia et al., 2021). However, when compared to a multi-layer perceptron (Simard et al., 2003) ($98.4\,\%$) or vanilla CNN

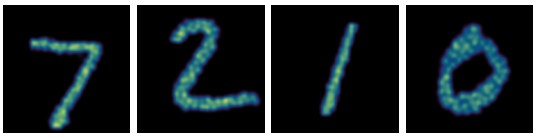

Figure 5: GM fitting examples of MNIST digits. 64 Gaussians were used to represent each input sample.

Table 1: ModelNet10 classification results of our method in comparison with PointNet and PointNet++. We show two variants of competitor training: 1., on a set of points that matches the memory footprint of the GM, and 2., trained on the same GM inputs. The number of Gaussian (G) and the number of points (P) are indicated in the header for each column.

		32 G / 106 P	*64 G / 213 P*	*128 G / 426 P*	*#Params*
Points	PointNet	91.3 %	92.0 %	92.2 %	3.4 M
	PointNet++	92.8 %	93.3 %	93.9 %	1.4 M
GM	PointNet	90.7 %	91.9 %	91.6 %	3.4 M
	PointNet++	91.8 %	92.1 %	92.4 %	1.4 M
	Ours	92.1 %	92.3 %	93.3 %	215 K

architectures (Lecun et al., 1998) (99.2 %), which more closely reflect the GMCN design we used, our method performs better. Compared to point-based methods, our network achieves competitive performance (PointNet (Qi et al., 2017a) 99.2 % and PointNet++ (Qi et al., 2017b) 99.5 %).

5.2 3D DATA CLASSIFICATION (MODELNET 10)

ModelNet10 (Zhirong Wu et al., 2015) is a data set used to measure 3D classification accuracy and consists of 3D models of different man-made objects. The data set contains 4.8 K different models from 10 different categories. We trained our network to classify ModelNet10 samples using the standard train/test splits. In order to fit the 3D data with a GM, we used the point clouds provided by Qi et al. (2017b), which were obtained by randomly sampling the surface of the 3D models. We then fit 128 Gaussians to these point clouds to generate the input for our network. Our trained model achieved an accuracy of 93.3 %, which is similar to other state-of-the-art classifiers: 94.0 % (Klokov & Lempitsky, 2017) or 95.7 % (Li et al., 2018a).

In Table 1, we again compare our method with PointNet (Qi et al., 2017a) and PointNet++ (Qi et al., 2017b), as they represent two well-established methods for point cloud processing. To enable a fair comparison with each point-based technique, we ran two variants: The first uses a point cloud as input, with a number of points equivalent to the memory footprint of our GM representation. The second uses the same GM inputs as our network, where weight and covariance matrix are processed as additional features for each point. Models are trained with various input sizes: 32 Gaussians (106 points), 64 Gaussians (213 points), and 128 Gaussians (426 points). We found that our method outperforms PointNet on all experiments using an order of magnitude fewer parameters. It also achieves similar performance to the point-based hierarchical architecture PointNet++ using five times fewer parameters. Our method outperforms both architectures when processing GMs directly.

5.3 ABLATION STUDIES

In this section, we discuss additional experiments carried out to validate the individual elements of our network. For these ablation studies, we use the ModelNet10 data set in all experiments.

Network depth. First, we evaluate the network's performance wrt. the depth of our GMCN to determine the optimal number of layers. Table 2 shows the classification accuracy on the ModelNet10 data set for different models with varying numbers of convolution layers. We confirmed that GMCN can benefit from additional layers; however, the accuracy stops increasing once we reach five layers.

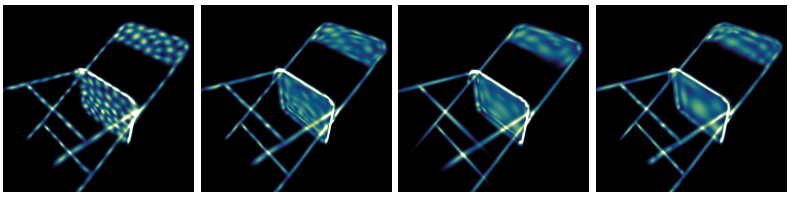

k-means init *k-means init + EM* *random init + EM* *Eckart*

Figure 6: GM fitting examples of a ModelNet object with 128 Gaussians for k-means and EM algorithms and 125 Gaussians for Eckart et al. (2016b). The k-means initialization method does not produce smooth surface fittings, but Gaussians have uniform covariances. EM with k-means produces results that are relatively sharp on edges and smooth on surfaces. EM with random initialization and Eckart produces even smoother surfaces.

Table 2: Accuracy and training time on the ModelNet10 data set for our model wrt. the number of layers. Our network benefits from additional layers. However, accuracy saturates after five layers. While training times in our proof-of-concept system are not competitive, GMCNs leave much room for optimizations in future work.

	1	2	3	4	5	6
Accuracy	72.5 %	89.4 %	91.2 %	92.0 %	92.6 %	92.3 %
Training time	0.5h	2h	5h	10h	21h	41h

Gaussian mixture fitting. We evaluated the two proposed fitting algorithms (Section 4.1) used after each convolution layer. Three different reduction variants were tested: modified EM, TreeHEM with $T = 2$ and 4 Gaussians per node. Table 3 shows the results of these methods in terms of fitting error in the first three layers and the accuracy of the model when using 64 and 128 Gaussians as input, respectively. TreeHEM obtains a lower fitting error in most of the layers when compared to the EM algorithm. Moreover, the tree-based method also requires less memory during training compared to EM, which runs out of memory when trained on inputs represented by 128 Gaussians. However, EM obtains a slightly higher classification accuracy for 64 input Gaussian. Out of the two TreeHEM variants, the two-Gaussian approach performs better in fitting error and classification accuracy.

Input data fitting. Lastly, we evaluate how the model is affected by the different algorithms used to fit the input data. We compare four different methods: k-means initialization plus one single step of EM (*k-means*), k-means initialization plus multiple EM steps (*k-means+EM*), random initialization plus multiple EM steps (*rand+EM*), and the method proposed by Eckart et al. (2016b) (*Eckart*). Figure 6 shows the resulting GMs of the four different algorithms for two different models from ModelNet10. We see that *k-means* produces a set of Gaussians with relatively uniform shapes, but overall does not fit the data accurately. *Random init + EM* and *Eckart* can fit the model with high precision but also produces some blurred areas. *K-means init + EM* achieves the best representation of the four methods.

The resulting accuracy of our network for the four types of input GMs is reported in Table 4. *K-means* initialization achieves the best accuracy while *Eckart* performs worst. We believe these results can be explained by the uneven Gaussian covariance matrices present on methods such as *Eckart* and *rand+EM*.

Table 3: Evaluation of our proposed fitting algorithm. We find that TreeHEM achieves lower errors than the modified EM algorithm when fitting the output of different layers. Nonetheless, accuracy is similar. Moreover, we can see that the EM algorithm runs out of memory when using 128 input Gaussians.

	Fit err. (Layer)			# Gaus.		Memory		Training time	
	1	2	3	64	128	64	128	64	128
EM	0.45	0.50	0.36	92.2 %	n/a	2.5GB	n/a	6h	n/a
Tree (4)	0.35	0.22	0.25	91.3 %	92.9 %	1.6GB	6.8GB	5h	22h
Tree (2)	0.36	0.21	0.22	92.0 %	93.4 %	1.3GB	5.6GB	4h	19h

Table 4: Accuracy of our model on the ModelNet10 data set for input GM generated using different algorithms. Results show that *k-means* produces the best accuracy, while more advanced methods that generate uneven covariance matrices, such as Eckart et al. (2016b), reduce the classification accuracy of the network.

k-means	*k-means+EM*	*rand+EM*	*Eckart*
93.3 %	92.1 %	92.8 %	91.0 %

6 Discussion and conclusion

To the best of our knowledge, we are the first to propose a deep learning method based on the analytical convolution of GMs with unconstrained positions and covariance matrices. We have outlined a complete architecture for the task of general-purpose deep learning, including convolution layers, a transfer function, and pooling. Our evaluation demonstrates that this architecture is capable of obtaining competitive results on well-known data sets. Its ability to avoid the curse of dimensionality seems evident: even in comparison with sparse, point-based methods, it achieves comparable accuracy using between $5\times$ and $10\times$ fewer parameters. Hence, we consider our architecture as a promising candidate for applications that require higher-dimensional input or compact networks.

Limitation and future work. Currently, the most significant bottleneck to limit the universal application of our work is the—unavoidable—fitting process. As reflected by the results in Table 2, the implied computation time limits the size of GMCNs that can be trained with consumer-grade hardware in an appropriate amount of time. The simple GMCN architecture presented in Section 5 is insufficient for achieving competitive results on more complex tasks, such as classification on ModelNet40 and FashionMNIST data sets (87% and 86% accuracy, respectively).

However, early experiments have shown that performance can be drastically improved by embedding a fitting step in the convolution stage. Specifically, we can use an on-the-fly convolution of the positions to construct an auxiliary tree data structure, in a manner similar to Section 4.1. The resulting tree is then used to perform a full convolution and fitting in one stage. We have identified highly parallel algorithms for the required steps and confirmed that applying these optimizations to our methods can significantly reduce memory traffic and improve computation times by more than an order of magnitude.

We further conjecture that the achieved prediction quality with our architecture is currently limited by fitting accuracy. This could be addressed by sampling the GM and performing one or two EM steps on these samples. Doing so should become feasible once the number of Gaussians is brought down using the convolution fitting step described above. Presumably, even a slight increase in accuracy would enable us to achieve state-of-the-art results on all tested use cases.

Additional extensions to raise the applicability of GMCNs would be the introduction of transposed convolution, as well as skip connections (Ronneberger et al., 2015). We expect that these tasks could be solved with a reasonable amount of additional effort. We hope to enable novel solutions for 3-dimensional problems with these extended GMCNs in future work, such as hole-filling for incomplete 3D scans or learning physical simulations for smoke and fluids.

Reproducibility

The source code for a proof-of-concept implementation is provided in the supplemental material (Github after deanonymization).

Acknowledgments

References

Eman Ahmed, Alexandre Saint, Abd El Rahman Shabayek, Kseniya Cherenkova, Rig Das, Gleb Gusev, Djamila Aouada, and Bjorn Ottersten. A survey on Deep Learning Advances on Different 3D Data Representations. 1(1):1–35, 2018. URL http://arxiv.org/abs/1808.01462.

Matan Atzmon, Haggai Maron, and Yaron Lipman. Point convolutional neural networks by extension operators. *ACM Transactions on Graphics*, 37(4), 2018. ISSN 15577368. doi: 10.1145/3197517.3201301.

Alexandre Boulch. ConvPoint: continuous convolutions for point cloud processing. pp. 1–12, 2019. URL http://arxiv.org/abs/1904.02375.

David S Broomhead and David Lowe. Radial basis functions, multi-variable functional interpolation and adaptive networks. Technical report, Royal Signals and Radar Establishment Malvern (United Kingdom), 1988.

Adam Byerly, Tatiana Kalganova, and Ian Dear. A branching and merging convolutional network with homogeneous filter capsules, 2020.

A. P. Dempster, N. M. Laird, and D. B. Rubin. Maximum Likelihood from Incomplete Data Via the EM Algorithm . *Journal of the Royal Statistical Society: Series B (Methodological)*, 39(1), 1977. doi: 10.1111/j.2517-6161.1977.tb01600.x.

Ben Eckart, Kihwan Kim, Alejandro Troccoli, Alonzo Kelly, and Jan Kautz. Accelerated generative models for 3D point cloud data. *Proceedings of the IEEE Computer Society Conference on Computer Vision and Pattern Recognition*, 2016-Decem:5497–5505, 2016a. ISSN 10636919. doi: 10.1109/CVPR.2016.593.

Benjamin Eckart, Kihwan Kim, Alejandro Troccoli, Alonzo Kelly, and Jan Kautz. Accelerated generative models for 3D point cloud data. In *Proceedings of the IEEE Conference on Computer Vision and Pattern Recognition*, pp. 5497–5505, 2016b.

Yulan Guo, Hanyun Wang, Qingyong Hu, Hao Liu, Li Liu, and Mohammed Bennamoun. Deep Learning for 3D Point Clouds : A Survey. *IEEE Transactions on Pattern Analysis and Machine Intelligence*, pp. 1–24, 2019. URL https://doi.org/10.1109/TPAMI.2020.3005434.

Pedro Hermosilla, Tobias Ritschel, Pere Pau Vázquez, Àlvar Vinacua, and Timo Ropinski. Monte Carlo convolution for learning on non-uniformly sampled point clouds. *SIGGRAPH Asia 2018 Technical Papers, SIGGRAPH Asia 2018*, 37(6), 2018. doi: 10.1145/3272127.3275110.

Wenzel Jakob, Christian Regg, and Wojciech Jarosz. Progressive Expectation-Maximization for Hierarchical Volumetric Photon Mapping. *Computer Graphics Forum*, 30(4):1287–1297, jun 2011. ISSN 01677055. doi: 10.1111/j.1467-8659.2011.01988.x. URL http://doi.wiley.com/10.1111/j.1467-8659.2011.01988.x.

Shuiwang Ji, Wei Xu, Ming Yang, and Kai Yu. 3D Convolutional Neural Networks for Human Action Recognition. *IEEE Transactions on Pattern Analysis and Machine Intelligence*, 35(1):221–231, jan 2013. ISSN 0162-8828. doi: 10.1109/TPAMI.2012.59. URL http://ieeexplore.ieee.org/document/6165309/.

Roman Klokov and Victor Lempitsky. Escape from cells: Deep kd-networks for the recognition of 3d point cloud models. In *2017 IEEE International Conference on Computer Vision (ICCV)*, 2017.

Alex Krizhevsky, Ilya Sutskever, and Geoffrey E. Hinton. ImageNet classification with deep convolutional neural networks. *Advances in Neural Information Processing Systems 25*, 25:1097—-1105, may 2012. ISSN 0001-0782. doi: 10.1145/3065386. URL https://dl.acm.org/doi/10.1145/3065386.

C. Lauterbach, M. Garland, S. Sengupta, D. Luebke, and D. Manocha. Fast BVH construction on GPUs. *Computer Graphics Forum*, 28(2):375–384, 2009. ISSN 01677055. doi: 10.1111/j.1467-8659.2009.01377.x.

Allan M. M. Leal. autodiff, a modern, fast and expressive C++ library for automatic differentiation. https://autodiff.github.io, 2018. URL https://autodiff.github.io.

Y. Lecun, L. Bottou, Y. Bengio, and P. Haffner. Gradient-based learning applied to document recognition. *Proceedings of the IEEE*, 86(11):2278–2324, 1998. ISSN 00189219. doi: 10.1109/5.726791. URL http://ieeexplore.ieee.org/document/726791/.

Jiaxin Li, Ben M. Chen, and Gim Hee Lee. So-net: Self-organizing network for point cloud analysis. In *2018 IEEE/CVF Conference on Computer Vision and Pattern Recognition*, 2018a.

Yangyan Li, Rui Bu, Mingchao Sun, Wei Wu, Xinhan Di, and Baoquan Chen. PointCNN: Convolution On χ-Transformed Points. *Advances in Neural Information Processing Systems*, 2018-Decem: 820–830, jan 2018b. ISSN 10495258. URL http://arxiv.org/abs/1801.07791.

Daniel Maturana and Sebastian Scherer. VoxNet: A 3D Convolutional Neural Network for real-time object recognition. In *2015 IEEE/RSJ International Conference on Intelligent Robots and Systems (IROS)*, pp. 922–928. IEEE, sep 2015. ISBN 978-1-4799-9994-1. doi: 10.1109/IROS.2015.7353481. URL http://ieeexplore.ieee.org/document/7353481/.

Vittorio Mazzia, Francesco Salvetti, and Marcello Chiaberge. Efficient-capsnet: Capsule network with self-attention routing. *arXiv preprint arXiv:2101.12491*, 2021.

Reinhold Preiner, Oliver Mattausch, Murat Arikan, Renato Pajarola, and Michael Wimmer. Continuous projection for fast L 1 reconstruction. *ACM Transactions on Graphics*, 33(4):1–13, 2014. ISSN 07300301. doi: 10.1145/2601097.2601172.

Charles R. Qi, Hao Su, Kaichun Mo, and Leonidas J. Guibas. PointNet: Deep Learning on Point Sets for 3D Classification and Segmentation. *The IEEE Conference on Computer Vision and Pattern Recognition (CVPR)*, 2017a. doi: 10.1109/CVPR.2017.16.

Charles R Qi, Li Yi, Hao Su, and Leonidas J Guibas. PointNet++: Deep Hierarchical Feature Learning on Point Sets in a Metric Space. (Nips), jun 2017b. doi: 10.1016/S0039-9140(96)02179-0. URL http://arxiv.org/abs/1706.02413.

Gernot Riegler, Ali Osman Ulusoy, and Andreas Geiger. OctNet: Learning deep 3D representations at high resolutions. In *Proceedings - 30th IEEE Conference on Computer Vision and Pattern Recognition, CVPR 2017*, volume 2017-Janua, 2017. ISBN 9781538604571. doi: 10.1109/CVPR.2017.701.

Olaf Ronneberger, Philipp Fischer, and Thomas Brox. U-Net: Convolutional Networks for Biomedical Image Segmentation. In *Medical Image Computing and Computer-Assisted Intervention – MICCAI 2015*, pp. 234–241, 2015. doi: 10.1007/978-3-319-24574-4_28. URL http://link.springer.com/10.1007/978-3-319-24574-4_28.

P.Y. Simard, D. Steinkraus, and J.C. Platt. Best practices for convolutional neural networks applied to visual document analysis. In *Seventh International Conference on Document Analysis and Recognition, 2003. Proceedings.*, 2003.

Hugues Thomas, Charles R. Qi, Jean-Emmanuel Deschaud, Beatriz Marcotegui, François Goulette, and Leonidas J. Guibas. KPConv: Flexible and Deformable Convolution for Point Clouds. apr 2019. URL http://arxiv.org/abs/1904.08889.

Nuno Vasconcelos and Andrew Lippman. Learning mixture hierarchies. *Advances in Neural Information Processing Systems*, pp. 606–612, 1999. ISSN 10495258.

Susana Vinga. Convolution integrals of Normal distribution functions. *Supplementary material to S.Vinga and JS.Almeida (2004) "Renyi continuous entropy of DNA sequences". J.Theor.Biol. 231(3):377–388*, 2004. URL http://web.ist.utl.pt/$\sim$susanavinga/renyi/convolution_normal.pdf.

Peng Shuai Wang, Yang Liu, Yu Xiao Guo, Chun Yu Sun, and Xin Tong. O-CNN: Octree-based convolutional neural networks for 3D shape analysis. In *ACM Transactions on Graphics*, volume 36, 2017. doi: 10.1145/3072959.3073608.

Yifan Xu, Tianqi Fan, Mingye Xu, Long Zeng, and Yu Qiao. SpiderCNN: Deep Learning on Point Sets with Parameterized Convolutional Filters. In *Computer Vision – ECCV 2018*, pp. 90–105. mar 2018. doi: 10.1007/978-3-030-01237-3_6. URL http://arxiv.org/abs/1803.11527http://link.springer.com/10.1007/978-3-030-01237-3_6.

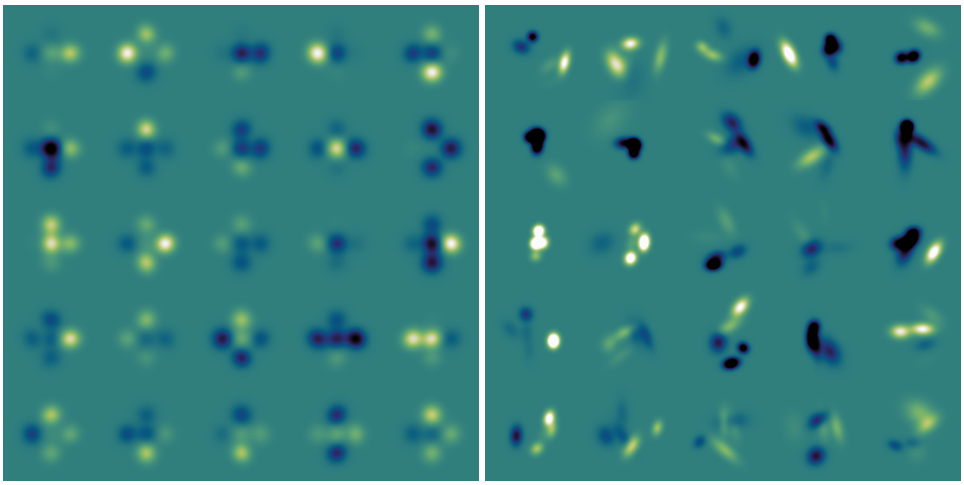

Initialization *After about 1 million training steps*

Figure 7: Convolution kernels of a 2d dataset. It is clearly visible, that all of the parameters (weights, positions and covariance matrices) adapt to the data, once training progresses.

Zhirong Wu, Shuran Song, Aditya Khosla, Fisher Yu, Linguang Zhang, Xiaoou Tang, and Jianxiong Xiao. 3D ShapeNets: A deep representation for volumetric shapes. In *2015 IEEE Conference on Computer Vision and Pattern Recognition (CVPR)*, pp. 1912–1920. IEEE, jun 2015. ISBN 978-1-4673-6964-0. doi: 10.1109/CVPR.2015.7298801. URL http://ieeexplore.ieee.org/document/7298801/.

A Kernel examples

Figure 7 shows examples of training kernels for a 2d dataset.

B Theoretical minimal memory footprint (and number of parameters)

In conventional CNNs, the convolution operation, that is "per-pixel kernel-sized window, element-wise multiplication, and sum", are usually built into one compact function, or CUDA kernel. Accordingly, intermediate results are never stored in memory. The proof-of-concept implementation described in this paper is not compact in the same way. The closed-form solution of the convolution with GMCNs yields a large number of intermediate output Gaussians, which are then greatly reduced in the fitting step before being forwarded to the next layer. The described prototype explicitly stores these intermediate results, making it easier to implement and explain. However, as outlined in Chapter 6, the integration of a fitting step directly into the convolution is possible with our approach, albeit more complex compared to conventional CNNs.

The purpose of this appendix is to provide formal equations and concrete examples to outline the theoretical minimum memory footprint of a GMCN and assess its overall potential for reducing memory consumption. For this, we made the following assumptions:

- Fitting is integrated into the convolution layer and produces a mixture with a specified number of Gaussians N_o. No fitting is performed if the specified number is equal to the number of Gaussians produced by the convolution.
- None of the modules (convolution / reduction fitting, transfer function fitting, pooling) contain caches.
- Programming code is not counted.
- Minimal storage for a 2d Gaussian requires 6 floats, and for a 3d Gaussian 10 floats.

Table 5: Minimal memory footprint for the network shown in Figure 1, using Equations 10, if $N_o = N_i$. The total number of Gaussians for each convolution module is given as G. Theoretical memory usage in megabytes is given in columns M_{2D} and M_{3D}, using 2d and 3d Gaussians, respectively.

B	F_i	F_o	N_i	N_o	N_p	N_k	K	D	G	M_{2D}	M_{3D}
32	1	8	128	128	64	5	40	49152	98384	2.25	3.75
32	8	16	64	64	32	5	640	49152	99584	2.28	3.80
32	16	32	32	32	16	5	2560	49152	103424	2.37	3.95
32	32	64	16	16	8	5	10240	49152	118784	2.72	4.53
32	64	10	8	8	4	5	3200	3840	14080	0.32	0.54

Table 6: Minimal memory footprint for network shown in Figure 1, using Equations 10, if implemented without combined convolution-fitting. The total number of Gaussians for each convolution module is given as G. Theoretical memory usage in megabytes is given in columns M_{2D} and M_{3D}.

B	F_i	F_o	N_i	N_o	N_p	N_k	K	D	G	M_{2D}	M_{3D}
32	1	8	128	640	64	5	40	180224	360528	8.25	13.75
32	8	16	64	2560	32	5	640	1327104	2655488	60.78	101.30
32	16	32	32	2560	16	5	2560	2637824	5280768	120.87	201.45
32	32	64	16	2560	8	5	10240	5259264	10539008	241.22	402.03
32	64	10	8	2560	4	5	3200	820480	1647360	37.71	62.84

Convolution module A convolution module has F_i input feature channels, F_o output feature channels, batch size is B, incoming data mixtures contain N_i Gaussians, kernels contain N_k Gaussians, the integrated convolution-fitting module is set to produce N_o Gaussians, and the module contains a pooling layer, which reduces the number of Gaussians to N_p. Memory of the incoming data is accounted towards the previous module. The minimal memory footprint in terms of Gaussians (G) is the sum of kernels (K), and data (D) times 2 (for the gradient):

$$\begin{aligned} K &= F_i F_o N_k \\ D &= B(F_o N_o + F_o N_p) \\ G &= 2(K + D). \end{aligned} \tag{10}$$

K can be used to compute the number of parameters of the given module by multiplying with the representation used.

Model The factors and results for the model used for our evaluation (shown in Figure 4) are given in Tables 5 and 6. Overall, if $N_o = N_i$ is used, the model has a theoretical minimal memory footprint of 434,256 total 3D Gaussians, which is less than 17 megabytes. In comparison, the proof-of-concept implementation presented in this paper has a theoretical use of 781 megabytes. In practice, it requires several times more, since it uses convenience data structures that were not exhaustively optimized.

C Comparison of least-squares solution and heuristic for ReLU fitting

In this section, we will compare a least-squares solution with our heuristic presented in Section 4.1 for the fitting of a transfer function.

The least-squares solution has to solve the following problem

$$A\boldsymbol{y} = \boldsymbol{t}, \tag{11}$$

where $\boldsymbol{t}_i = \varphi(\mathrm{gm}(D_i))$ are the target values at positions D, and A is a matrix:

$$A = \begin{pmatrix} \gamma_0(D_0) & \dots & \gamma_N(D_0) \\ \vdots & \ddots & \vdots \\ \gamma_0(D_N) & \dots & \gamma_N(D_N) \end{pmatrix}, \tag{12}$$

Table 7: Computation time for various fitting methods on a dataset containing 800 mixtures, 256 Gaussians each. `torch.linalg.pinv` and `torch.linalg.lstsq` were tested, both functions being able to solve our problem. However, `lstsq` does not compute a gradient in the current pytorch version and would be therefore unusable. But even if so, the timings are prohibitive. Our heuristic takes only 3.8 milliseconds.

$D =$	B	$concat(B, rand(N, k))$	$rand(4N, k)$
`torch.linalg.pinv`	10.2s	10.9s	11.3s
`torch.linalg.lstsq`	1.1s	1.5s	2.0s

with $\gamma_i(\boldsymbol{x}) = \frac{1}{\sqrt{(2\pi)^k \det(C)}} e^{-\frac{1}{2}(\boldsymbol{x}-B_i)^T \boldsymbol{C}_i^{-1}(\boldsymbol{x}-B_i)}$. B_i is the centroid, $\boldsymbol{C}_i$ the covariance of Gaussian i, N is the number of Gaussians, and k the number of dimensions (e.g., 2 or 3). In other words, A contains the evaluations of the mixture Gaussians with the weight set to one, on a set of points contained in D.

We evaluated several choices for D:

- $D = B$, evaluate the mixture at the centre points of its Gaussians
- $D = rand(M, k)$, positions within the domain
- $D = concat(B, rand(M, k))$, mixture centres and random positions within the domain

Figure 8 shows part of our test input, along with the result of our heuristic. After seeing the results in Figure 9 and timings in Table 7, we refrained from computing the RMSE and selected the heuristic for our network. The least-squares solution overshoots away from the sampling points, and the compute resources are several magnitudes higher compared to our heuristic.

The matrix A with choice $D = B$ can be of $rank(A) < N$, and therefore (non-pseudo) inversion methods are not applicable.

D Details on the dense fitting

(This section is still work in progress and will be updated before November 22.) The purpose of this step is to fit a transfer function, for example a ReLU. Our fitting method only computes new weights for the mixture. Position and covariance matrices of the Gaussians are not changed (see 4.1).

Accordingly, we give only equations for the new weights $\boldsymbol{a}''$, which are computed in 2 steps. The first step computes a coarse, or initial approximation to the target:

$$\boldsymbol{a}'_{\boldsymbol{i}} = \begin{cases} \boldsymbol{a}_{\boldsymbol{i}}, & \text{if } \boldsymbol{a}_{\boldsymbol{i}} > 0 \\ \epsilon, & \text{otherwise} \end{cases}, \tag{13}$$

where $\boldsymbol{a}_{\boldsymbol{i}}$ are the weights of the old mixture, and i runs through all Gaussians. This design has two reasons: We think that it is safer if the weights are positive only, which is guaranteed, since the second step will not introduce a negative sign. Negative weights themselves are not a problem for the GMCN architecture. However, the ReLU gives a function that is positive through all of the domain, and so should the fitting. That still does not conflict with negative weights as long as the sum is greater zero throughout the domain. But we look only at the evaluation at the Gaussian's centroids, and negative weights could cause the sum to become negative away from these evaluation points. Something similar happens when using a linear solver (Section C). As a side effect, reduction fitting becomes simpler if it does not have to deal with negative weights. Secondly, we want to scale the Gaussians (change the weight) as little as possible, therefore we do not initialize $\boldsymbol{a}'_{\boldsymbol{i}}$ simply to 1. The rational here is, that we want to retain the shape of the mixture as much as possible without looking at the positions and covariance matrices. As an example, take 2 Gaussians with the same centroid, one with a large variance and small weight, the other with a small variance and large weight. This would give a large Gaussian-shaped arch with a strong bump in the middle. Now, if we initialized the weights to one, the result at the centroid would be approximately correct, but the shape would change.

The new weights $\boldsymbol{a}''$ are then computed using a correction based on the transfer function

$$\boldsymbol{a}''_{\boldsymbol{i}} = \boldsymbol{a}'_{\boldsymbol{i}} \times \frac{\varphi\left(\mathrm{gm}(B_i, \boldsymbol{a}, B, \boldsymbol{C})\right)}{\mathrm{gm}(B_i, \boldsymbol{a}', B, \boldsymbol{C})}, \tag{14}$$

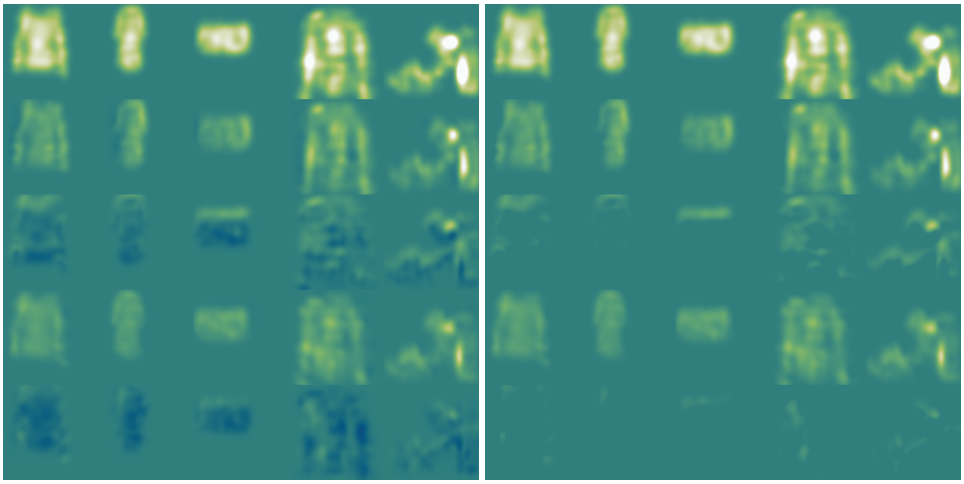

Input *Target (φ(input GM))*

Heuristic

Figure 8: Selection of the 800 Gaussian mixtures used for the evaluation of the ReLU fitting method.

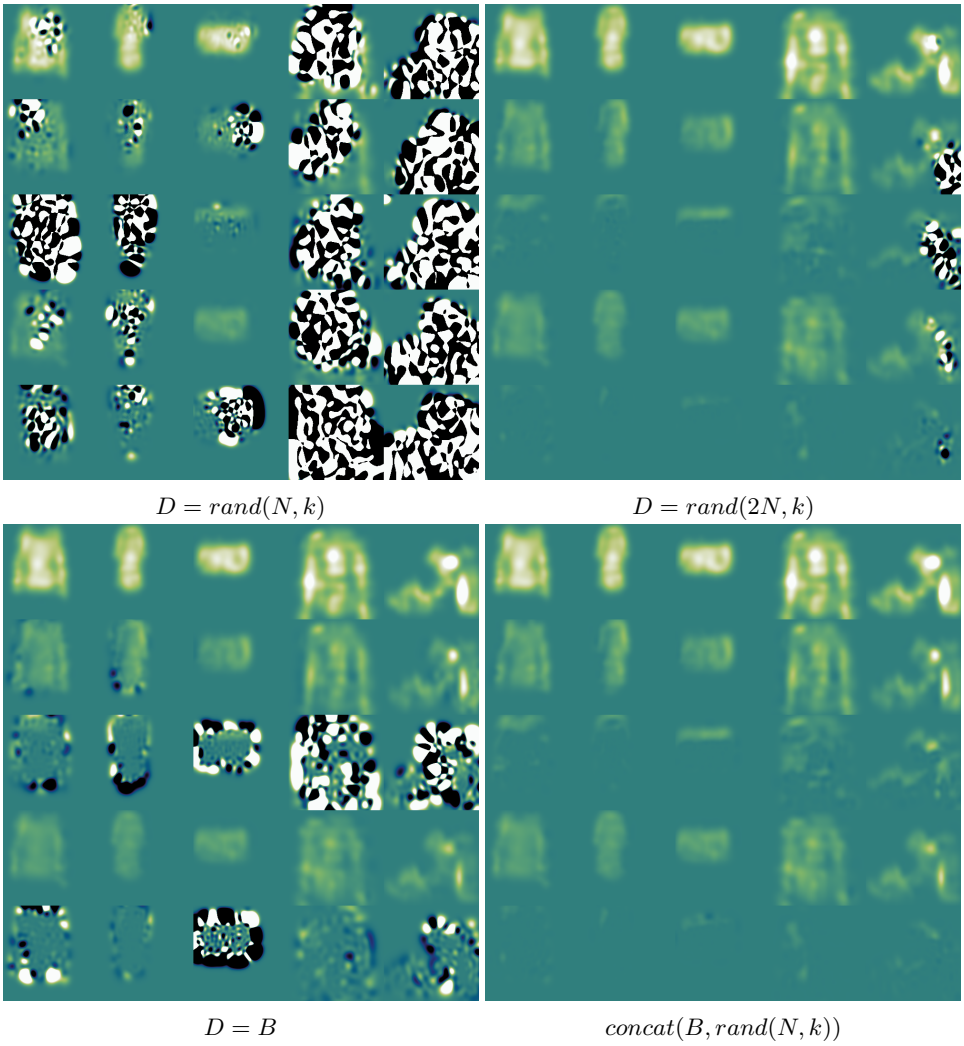

Figure 9: GM fitting using a least squares algorithm. We verified that the mixture fits the target at the sample positions, so the solution of the least-squares problem is correct in all cases. The mixture overshoots however and does not fit the ReLU well away from the sampling positions. Increasing the sample count, or selecting better samples helps, but even then there is no guarantee, that the mixture won't overshoot. `torch.linalg.lstsq` was used, but the results for `torch.linalg.pinv` are similar.

where B contains the positions, $\boldsymbol{C}$ the covariance matrices, and φ represents the ReLU. The fraction computes a correction factor for each Gaussian by evaluating the target function and the current approximation at the Gaussians centroid. This computation is $O(N^2)$ in the number of Gaussian components. In order to avoid storage of intermediate results and a large gradient tensor, we implemented the evaluation in a custom CUDA kernel. On the CPU it would be possible to trade accuracy for performance by ignoring contributions that are below a certain threshold, and using a tree based acceleration structure (e.g., a BVH). However, our tests showed, that this does not scale well on the GPU. The evaluation kernel is reasonably optimized, still, due to the large number of Gaussians, which can easily go into thousands, times the number of feature channels, times the batch size, these two evaluations account for roughly half of the overall training/test runtime.

In order to improve performance decisively, either the number of Gaussians would have to be reduced before this fitting step (e.g., during the convolution as outlined in the future work section), or a different algorithm used, or both.

E Details on the reduction step

(This section is still work in progress and will be updated before November 22.) The purpose of this step is to reduce the amount of data by fitting the *target* with a smaller mixture. It is applied after ReLU fitting, hence all weights are positive, and the mixture can be turned into a probability distribution easily. Therefore, probability based methods can be applied directly. In particular, it would be possible to sample the mixture and then use a expectation maximization (EM) algorithm. However, that would be prohibitively expensive for the given number of Gaussians.

In the following, we will first explain the hierarchical EM algorithm by Vasconcelos & Lippman (1999) and then show, how that maps to our TreeHEM algorithm.

Hierarchical EM Hierarchical EM starts with one Gaussian per point, which is the first level. In the successive levels $(l+1)$, a smaller mixture is fitted to the previous level (l). The new mixture needs to be initialized first, for instance by taking a random subset of the mixture in level l. In the E step, responsibilities are computed using (equations taken from Preiner et al. (2014))

$$r_{is} = \frac{\mathcal{L}(\Theta_s^{(l+1)}|\Theta_i^{(l)})w_s}{\sum_{s'} \mathcal{L}(\Theta_{s'}^{(l+1)}|\Theta_i^{(l)})w_{s'}}, \tag{15}$$

$$\mathcal{L}(\Theta_s^{(l+1)}|\Theta_i^{(l)}) = \left[g(\mu_i^{(l)}|\Theta_s^{(l+1)})e^{-\frac{1}{2}tr([\Sigma_s^{(l+1)}]^{-1}\Sigma_i^{(l)})}\right]^{\hat{w}_i}, \tag{16}$$

where $\hat{w}_i$ is the number of *virtual* samples. In the original paper, N points were fitted, so $\hat{w}_i = Nw_i$ corresponded to the number of points that Gaussian was modeling. We do not have points, so N becomes an implementation defined constant.

Afterwords, the M step can be taken:

$$w_s^{(l+1)} = \sum_i r_{is} w_i^{(l)} \tag{17}$$

$$w_{is} = r_{is} w_i / w_s^{(l+1)} \tag{18}$$

$$\mu_s^{(l+1)} = \sum_i w_{is} \mu_i^{(l)} \tag{19}$$

$$\Sigma_s^{(l+1)} = \sum_i w_{is} \left(\Sigma_i^{(l)} + (\mu_i^{(l)} - \mu_s^{(l+1)})(\mu_i^{(l)} - \mu_s^{(l+1)})^T\right), \tag{20}$$

where w, μ, and Σ are the weight, centroid, and covariance matrix, respectively, i is the index of the (larger) target mixture, s the index of the new mixture. In each level, only one iteration is taken (E and M step), and the algorithm continues with the next level. Preiner et al. (2014) propose a geometrical regularization, in which r_{is} is set to zero, if the Kullback-Leibler divergence between Gaussians i and s is larger than a certain threshold.

We were not able to use that method for reasons including difficult parallelization on the GPU, bad accuracy on our data, and bad performance, since every Gaussian needs to be tested against each other Gaussian.

TreeHEM We therefore developed the TreeHEM algorithm to improve on theses issues. In short, we build a spatial tree of the (larger) target Gaussians, and use it to localize the fitting, i.e., limit the fitting to a fixed-size subset of Gaussians in the vicinity.

The tree is built using the same algorithm, as is described by Lauterbach et al. (2009) for building bounding volume hierarchies of triangles (LBVH), minus the bounding boxes. In our case, we take the centroids, compute their Morton code, and use it to sort the mixture. This puts the Gaussians on a Z-order curve. It is then possible to build a tree in parallel by looking at the bit-pattern of the sorted Morton codes. Please look at the excellent paper from Lauterbach et al. for more details.

Storing the indices of children and parents in the tree allows us to traverse bottom-up and top-down.

The tree is traversed twice. In the first, bottom-up, pass we collect and fit Gaussians, and then store them in a cache with up to T Gaussians in the tree nodes. Bottom-up traversal is implemented in a parallel way, the first thread entering simply exits, and the second does the work. First, the Gaussians from the caches of the two children are collected, resulting in up to $2T$ Gaussians. If the children are leaves, or not yet full, then that number can be below T, in which case they are written into the cache. Otherwise T new Gaussians are fitted to the collected ones, stored in the cache, and traversal continues until reaching the root node.

For the fitting, we first select T initial Gaussians from the $2T$ collected ones. This is done by dividing the $2T$ Gaussians into T clusters. From each cluster, the Gaussian with largest weight is selected, giving T initial Gaussians. The rational is to try selecting the most important Gaussians without overlap. We then use Equations 15–20 to compute the fitting, where we set $l + 1$ to the initial mixture explained just now, and l to the target mixture consisting of $2T$ Gaussians.

At this point we have a tree, with T Gaussians in each node, that fit their children. In the second, top-down, pass we look to select N/T nodes that best describe the target mixture, where N is the number of Gaussians in the fitting. This was implemented as a greedy approach with a single thread per mixture (which is not a problem as the kernel only traverses the very top of the tree). All selected nodes are stored in an vector, that only contains the root node at the beginning. In each iteration, we search through the vector and select the node with largest mass (integral of Gaussians, i.e., sum of weights) and replace it with its two children. The iteration terminates once we selected N/T nodes. Finally, we go through these nodes, and copy the Gaussians from the cache into the destination tensor.

Gradient computation Since all of the above is implemented in a custom CUDA kernel, we do not have the usual automatic gradient computation. Therefore we had to compute the gradient manually. We implemented unit tests of our manual gradient against a gradient computed by the autodiff C++ library (Leal, 2018).

F Application of the ReLU to each Gaussian individually

(This section is still work in progress and will be updated before November 22.) Repeatedly the question came up, whether the ReLU fitting could be simplified by applying the transfer function directly in parameter space, i.e., on the weight vector. In other words, whether an approximation of the Gaussians by Diracs for the purpose of activation would be a possible solution.

Unfortunately that is not the case. Currently, if a negative Gaussian is on top of a positive one, then the negative would reduce the contribution of the positive one. The positive one could even disappear. This would not be possible, if the ReLu would be applied directly. All negative Gaussians would be cut away, while the positive ones would simply pass through. Effectively, this would disable the nonlinearity, and make the network only capable of separating 2 classes using a hyperplane.

G Complete results

(This section is still work in progress and will be updated before November 22.) If nothing else given, then the tables show the test accuracy as shown in TensorBoard with the smoothing set to 0.9. Times shown are for training on an NVIDIA GeForce 2080ti, without fitting of the input data. The network notation is *number of feature channels* / *number of fitted Gaussians* - next convolution-fitting module.

Table 8: ModelNet10 with TreeHem($T = 2$) fitting, batch size 14, testing network lengths.

epochs:	50	60	kernels	params	mem	time
1/128 - 8/64 - 16/32 - 32/16 - 64/8 - 128/4 - 10	92.22	92.30	12168	790921	5.9GB	41h 22m
1/128 - 8/64 - 16/32 - 32/16 - 64/8 - 10	92.44	92.61	3336	216841	3.4GB	21h 22m
1/128 - 8/64 - 16/32 - 32/16 - 10	91.83	91.99	968	62921	1.6GB	10h 10m
1/128 - 8/64 - 16/32 - 10	91.06	91.17	296	19241	0.7GB	4h 49m
1/128 - 8/64 - 10	89.37	89.36	88	5721	0.3GB	2h 6m
1/128 - 10	74.73	72.45	10	651	0.3GB	0h 36m

Table 9: ModelNet10 with TreeHem($T = 2$) fitting, batch size 21, testing number of input Gaussians.

epochs:	60	kernels	params
1/128 - 8/64 - 16/32 - 32/16 - 64/8 – 10	92.78	3336	216841
1/64 - 8/64 - 16/32 - 32/16 - 64/8 – 10	92.28	3336	216841
1/32 - 8/32 - 16/32 - 32/16 - 64/8 – 10	92.09	3336	216841
1/16 - 8/16 - 16/16 - 32/16 - 64/8 – 10	89.91	3336	216841
1/16 - 8/8 - 16/4 - 32/2 - 64/2 – 10	90.17	3336	216841
1/32 - 8/64 - 16/32 - 32/16 - 64/8 – 10	91.44	3336	216841
1/16 - 8/64 - 16/32 - 32/16 - 64/8 – 10	90.92	3336	216841

Table 10: ModelNet10 *1/64 - 8/32 - 16/16 - 32/8 - 10*, batch size 21, testing fitting accuracy. We show RMSE of the fitting against the target (ground truth).

epochs:	**50**	**60**
MEM	92.18	92.22
TreeHEM (T=2)	91.95	91.95
TreeHEM (T=4)	91.29	91.31

	convolution layer 1		
	all	**ReLU**	**reduction**
MEM	0.4457	0.1639	0.2653
TreeHEM (T=2)	0.359	0.2253	0.1144
TreeHEM (T=4)	0.3487	0.2204	0.1159

	convolution layer 2		
	all	**ReLU**	**reduction**
MEM	0.4991	0.1433	0.2694
TreeHEM (T=2)	0.208	0.1031	0.07176
TreeHEM (T=4)	0.223	0.1104	0.08062

	convolution layer 3		
	all	**ReLU**	**reduction**
MEM	0.3582	0.1792	0.08425
TreeHEM (T=2)	0.2206	0.1346	0.04692
TreeHEM (T=4)	0.2461	0.1259	0.0707

	convolution layer 4		
	all	**ReLU**	**reduction**
MEM	n/a	n/a	n/a
TreeHEM (T=2)	n/a	0.5069	n/a
TreeHEM (T=4)	n/a	0.538	n/a

Table 11: ModelNet10 *1/128 - 8/64 - 16/32 - 32/16 - 64/8 - 10* (more Gaussians), batch size 21, testing fitting accuracy. We show RMSE of the fitting against the target (ground truth).

epochs:	**50**	**60**
MEM		
TreeHEM (T=2)	93,21	93,43
TreeHEM (T=4)	92,90	92,93

	convolution layer 1		
	all	**ReLU**	**reduction**
MEM	out of memory		
TreeHEM (T=2)	0,3391	0,2177	0,09483
TreeHEM (T=4)	0,3477	0.228	0,1011

	convolution layer 2		
	all	**ReLU**	**reduction**
MEM	out of memory		
TreeHEM (T=2)	0,2116	0,1121	0,06886
TreeHEM (T=4)	0,1859	0,1032	0,06498

	convolution layer 3		
	all	**ReLU**	**reduction**
MEM	out of memory		
TreeHEM (T=2)	0,2085	0,1415	0,03345
TreeHEM (T=4)	236	0,1524	0,04677

	convolution layer 4		
	all	**ReLU**	**reduction**
MEM	out of memory		
TreeHEM (T=2)	0,1204	0,07247	0,02597
TreeHEM (T=4)	0,1559	0,07643	0,04492

Table 12: ModelNet10 *1/128 - 8/64 - 16/32 - 32/16 - 64/8 - 10*, batch size 21, testing different methods for input fitting.

epochs:	**5**	**50**	**60**
kmeans + em	82,36	92,72	92,81
random + em	80,42	91,94	92,13
eckart	80,48	90,82	91,04
kmeans	84,06	93,11	93,29

Table 13: ModelNet40, testing different configurations, but can't do much due to long runtime.

epochs:	**50**	**60**	**batch**	**kernels**	**params**	**time**
1/128 - 8/64 - 16/32 - 32/16 - 64/8 - 128/4 - 40	77,84	77,82	14	16008	1040521	4d 23h 17m
1/128 - 8/64 - 16/32 - 32/16 - 64/8 - 40	87,35	87,62	14	5256	341641	2d 14h 57m
1/128 - 8/64 - 16/32 - 32/16 - 64/8 - 40	86,65	87,01	21	5256	341641	2d 12h 7m